

Irradiation responses and defect behavior of single-phase concentrated solid solution alloys

Tengfei Yang^{b)} and Congyi Li^{b)}

Department of Nuclear Engineering, University of Tennessee, Knoxville, Tennessee 37996, USA

Steven J. Zinkle^{a)}

Department of Nuclear Engineering, University of Tennessee, Knoxville, Tennessee 37996, USA; and Materials Science and Technology Division, Oak Ridge National Laboratory, Oak Ridge, Tennessee 37831, USA

Shijun Zhao and Hongbin Bei

Materials Science and Technology Division, Oak Ridge National Laboratory, Oak Ridge, Tennessee 37831, USA

Yanwen Zhang

Materials Science and Technology Division, Oak Ridge National Laboratory, Oak Ridge, Tennessee 37831, USA; and Department of Nuclear Engineering, University of Tennessee, Knoxville, Tennessee 37996, USA

(Received 15 April 2018; accepted 24 July 2018)

Single-phase concentrated solid solution alloys (SP-CSAs) are newly emerging advanced structural materials, which are defined as multiprincipal element solid solutions. SP-CSAs with more than four components in equimolar or near-equimolar ratios are also referred to as high-entropy alloys due to their high configurational entropy. SP-CSAs are potential structural materials in advanced nuclear energy systems due to their attractive mechanical properties. Therefore many investigations have been carried out to study the irradiation-induced structural damage and defect behavior in SP-CSAs. This paper reviews recent experimental results on the irradiation responses of various SP-CSAs, focusing on the accumulation of irradiation-induced structural damage, void swelling resistance, and solute segregation behavior. In addition, the characteristic defect behavior in SP-CSAs derived from *ab initio* and molecular dynamics simulations, as well as the challenges in the applications of SP-CSAs for the nuclear energy systems are briefly discussed.

I. INTRODUCTION

Nuclear power accounts for more than 11% of world electricity production and is a clean energy source with near-zero carbon emission.^{1,2} On the other hand, the long-term reliability and safety of nuclear power systems depend on the integrity of its structural materials.³ For future advanced fission and fusion reactors, the core structure materials are generally exposed to the aggressive environments, including high temperatures, large time-varying stresses, chemically reactive environments, and intense neutron irradiation.⁴ All of these attributes place demanding requirements on the structural materials used in advanced reactors. Energetic neutrons produced from nuclear fission or fusion damage the material by inducing significant atomic displacements and creating point defects or defect clusters. In some cases, atoms will be displaced from their initial lattice positions up to 200 times, producing a very high concentration of

vacancies and self-interstitial atoms. The evolution of irradiation-induced displacement damage can result in the complex and deleterious microstructural and microchemical evolutions, including the accumulation of extended vacancy and interstitial-type defect clusters, void swelling, solute segregation at defects or grain boundaries, as well as precipitation. These effects can seriously degrade the material performances and reduce its useful lifetime. Since the core structural materials must maintain both mechanical performance, such as strength, ductility, fracture toughness, and dimensional stability (against creep and void swelling) under high irradiation flux and high temperature environment,⁵ it is crucial to develop new irradiation-tolerant structural materials for advanced reactors.

Several guidelines have been proposed for designing advanced irradiation resistant materials.^{6,7} The potential candidates include the newly emerging high-entropy alloys (HEAs) and single-phase concentrated solid solution alloys (SP-CSAs). Different from conventional alloys composed of one principal element, SP-CSAs are composed of multiple principal elements. Many HEAs and SP-CSAs with excellent mechanical properties have

^{a)}Address all correspondence to this author.
e-mail: szinkle@utk.edu

^{b)}These authors contributed equally to this work.
DOI: 10.1557/jmr.2018.285

been identified. For example, FeCoCrMnNi and CoCrNi exhibit exceptional damage-tolerance at cryogenic temperatures, and the tensile strength and failure strains of CoCrNi at room temperature can reach ~ 1 GPa and $\sim 70\%$, respectively.^{8,9} Otto et al.¹⁰ studied the tensile properties and microstructures of FeCoCrMnNi at different temperatures ranging from 77 to 1073 K, and it was found that yield strength, ultimate tensile strength, and elongation to fracture all increased with decreasing temperature, which is attributed to the nanotwinning deformation mechanisms in low temperatures. In general, SP-CSAs based on 3d transition metals show high strength and ductility. Furthermore, HEAs and SP-CSAs can also possess high hardness, great fatigue resistance, good oxidation resistance, and age-softening resistance.^{11–19} Based on experimental measurements of diffusion parameters, SP-CSAs are also believed to have sluggish diffusion kinetics than conventional alloys due to the high lattice distortion.²⁰

While extensive studies have been conducted on investigating SP-CSA's favorable mechanical properties, the study of irradiation effects in SP-CSAs is only in a nascent stage. On the other hand, results from preliminary research indicate that SP-CSAs have improved tolerance to irradiations,^{21,22} suggesting that SP-CSAs can be a promising material for nuclear power applications. In this paper, we present the current understanding of irradiation effects in SP-CSAs by reviewing previous experimental results, focusing on the accumulation of irradiation-induced structural damage at room temperature, elevated temperature void swelling resistance, phase stability, segregation behavior, and evolution of irradiation-induced defects with composition and temperature. Following that, the characteristic defect behavior in SP-CSAs derived from *ab initio* and molecular dynamics (MD) studies, and the prospect of research in this field will be briefly discussed.

II. IRRADIATION RESPONSES OF SP-CSAs

A. Irradiation-induced structural damage at room temperature

Both the evolution of displacement cascades and defect migration can influence the irradiation-induced structural damage at room temperature. The irradiation-induced defects and defect clusters produced at room temperature are relatively simple as compared with high temperature irradiation; room temperature irradiations generally do not result in the formation of voids, precipitates, and other large and complex defect clusters at low dose. Therefore, the effect of alloy composition on the formation of defects and accumulation of irradiation-induced structural damage can be readily studied and compared at room temperature.

It is well established that solid solution alloying additions can suppress defect cluster accumulation and

loss of tensile elongation compared to pure metals following neutron or energetic ion irradiation near room temperature. For example, addition of >5 at.% Al, Ga, Ge, or Ni solid solution solute to copper resulted in dramatic reduction of defect cluster formation with diameters >5 nm in copper irradiated with neutrons near room temperature, whereas the alloying effect on formation of smaller “black spot” defects was minor.^{23,24} In general, the fine-scale “black spot” defect clusters in bulk irradiated FCC metals have been analyzed to vacancy-type whereas most defect clusters larger than ~ 5 nm are interstitial-type.²⁵ The fundamental mechanism for the formation of the fine-scale “black spot” defect clusters (typical sizes <5 nm) during energetic particle irradiation has been reported to be associated with athermal collapse of the vacancy-rich core of displacement cascades in both pure metals and solid solution alloys, although the detailed geometric configuration of these defect clusters depends on the solute and parameters such as stacking fault energy.^{24–27} Similarly, the visible defect cluster density and radiation-induced reduction in tensile ductility was significantly lower in Type 316 stainless steel (Fe–17Cr–13Ni–2Mo–2Mn) compared to pure Ni following neutron irradiation to 0.01–1 dpa near room temperature.²⁸

Recent studies have utilized multiple characterization techniques to compare the accumulation of irradiation-induced structural damage at room temperature in three face-centered cubic SP-CSAs and Ni following irradiation with 3 MeV Au and 1.5 MeV Ni at various fluences.²¹ Rutherford backscattering spectra and channeling (RBS-C) results show that the accumulation of structural damage is suppressed with increasing compositional complexity (the number of principal elements). Ni exhibits the highest structural disorder (backscattering yield) as compared with NiCo and NiFe under irradiation of 3 MeV Au [as shown in Fig. 1(a)]; while quaternary alloy NiCoFeCr exhibits the lowest structural disorder as compared with Ni and NiFe under irradiation of 1.5 MeV Ni [as shown in Fig. 1(b)]. TEM characterizations found that Ni has a higher average defect size than NiFe and NiCo, which was attributed to the suppression of interstitial motion and/or enhanced interstitial cluster nucleation due to the solute additions.²⁹

Granberg et al. further investigated the mechanism of irradiation damage suppression in SP-CSAs by combining experimental and modeling efforts.³⁰ MD simulation results reveal that the sequence of average defect sizes is Ni $>$ NiFe $>$ NiCoCr while the sequence of defect density is NiCoCr $>$ NiFe $>$ Ni [as shown in Figs. 2(a) and 2(b)]. The simulation results are qualitatively consistent with the TEM observations of ion irradiated-Ni, NiFe, and NiCoCr. By separately analyzing the mobility of edge dislocations in these materials, it is found that lattice distortion, which is a main characteristic of HEAs,

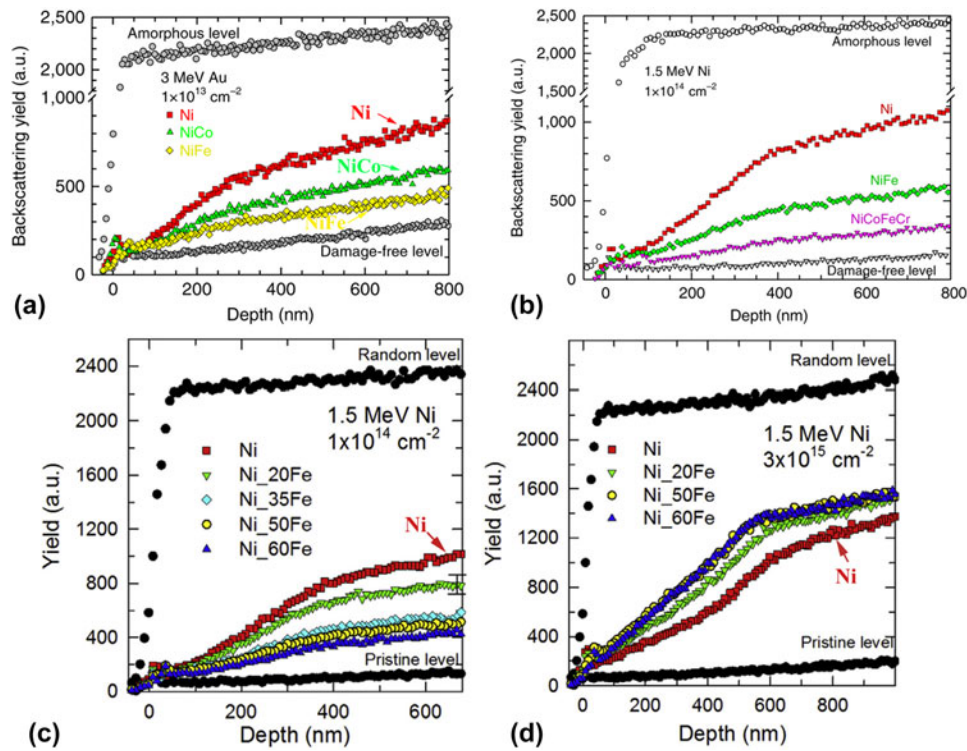


FIG. 1. RBS-C results of (a) Ni, NiCo, and NiFe irradiated with 3 MeV Au at $1 \times 10^{13} \text{ cm}^{-2}$ (Ref. 21) (reprinted with permission from Ref. 21; <https://creativecommons.org/licenses/by/4.0/legalcode>); (b) Ni, NiFe, and NiCoFeCr irradiated with 1.5 MeV Ni at $1 \times 10^{14} \text{ cm}^{-2}$ (Ref. 21) (reprinted with permission from Ref. 21; <https://creativecommons.org/licenses/by/4.0/legalcode>). RBS-C results of $\text{Ni}_x\text{Fe}_{1-x}$ ($0 < x < 60 \text{ at.}\%$) irradiated with 1.5 MeV Ni at (c) $1 \times 10^{14} \text{ cm}^{-2}$ and (d) $3 \times 10^{15} \text{ cm}^{-2}$ (Ref. 31) (reprinted with permission from Ref. 31).

can restrain the dislocation movement in the SP-CSAs. Therefore, the dislocations in the NiFe and NiCoCr are less likely to grow, resulting in the smaller damage structures and higher defect densities.

Furthermore, the irradiation responses of nonequiatom SP-CSAs were also studied to understand the effects of chemical complexity, including the number, type, and concentration of alloying elements, on defect dynamics and irradiation tolerance. Jin et al. compared the irradiation-induced structural damage in single crystalline $\text{Ni}_x\text{Fe}_{1-x}$ ($0 < x < 60 \text{ at.}\%$) alloys over a wide range of fluences from 3×10^{13} to $3 \times 10^{16} \text{ cm}^{-2}$ at room temperature.³¹ Based on the RBS-C measurements, it was found that the accumulation of irradiation-induced structural damage is restrained with increasing Fe concentration at low fluence regime [as shown in Fig. 1(c)]. MD simulations also obtained similar results that the addition of Fe can efficiently decrease the number of surviving interstitials in $\text{Ni}_x\text{Fe}_{1-x}$ alloys [as shown in Fig. 2(c)]. With increasing fluence, however, the irradiation-induced structural damage measured by RBS-C reaches a saturation. The saturation structural damage is essentially increased with increasing Fe concentration [as shown in Fig. 1(d)], which means that binary Ni_xFe can reach a higher structural damage level than Ni at high fluences and the saturation structural

damage of concentrated alloys is higher than that of dilute solid solutions. It should be noted that atom probe tomography (APT) was also used to characterize the compositional homogeneity of Ni_xFe alloys before and after ion irradiation. No irradiation-induced compositional segregation and precipitation was observed and the Ni_xFe alloys still remain a homogeneous distribution of elements, even at high fluences. This is consistent with other experimental results that the SP-CSAs can retain the compositional homogeneity under room temperature irradiation.

Lu et al.³² studied the irradiation-induced structural damage and defects in single crystalline Ni, NiCo, and FeNi at room temperature. They reported the depth range of irradiation-induced structural damage far exceed the depth range predicted by the SRIM, and the irradiation-induced defect clusters in Ni show a larger depth range than NiCo and NiFe, which suggests that mobilities of defects in the SP-CSAs are significantly lower than that of Ni.

Several basic conclusions regarding the irradiation response of SP-CSAs at room temperature can be drawn based on the above experimental results. First, SP-CSAs retain compositional homogeneity during room temperature irradiation; no sign of phase separation/decomposition or ordering is observed. Second, SP-CSAs exhibit a better

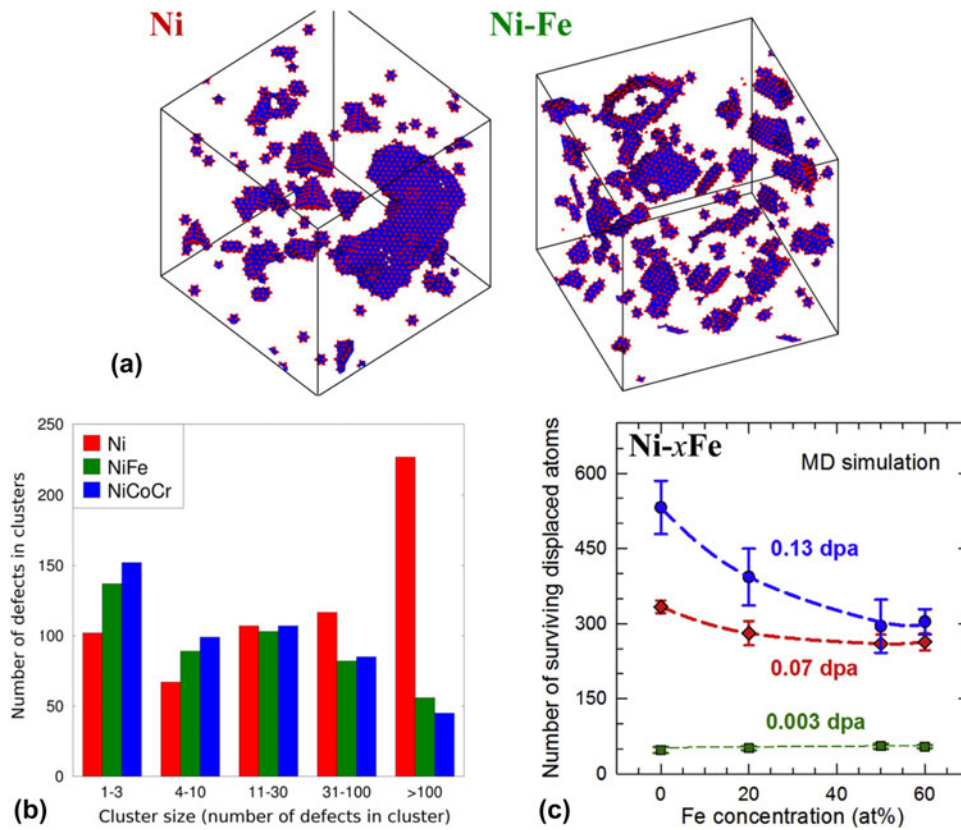


FIG. 2. MD simulation results showing (a) defect structures in Ni and NiFe at a dose of 0.5 dpa and (b) the distributions of defect cluster sizes in Ni, NiFe, and NiCoCr at the dose from ~ 0.4 dpa to the end³⁰ (reprinted with permission from Ref. 30; <https://creativecommons.org/licenses/by/3.0/legalcode>); (c) the number of surviving displaced atoms as a function of Fe concentration in the Ni-xFe alloys at three different doses.³¹ (reprinted with permission from Ref. 31).

irradiation tolerance than Ni at low fluences; the accumulation of irradiation-induced structural damage is slower in SP-CSAs. However, the SP-CSAs show a higher saturation structural damage than Ni at high fluences. Third, both MD and TEM results suggest that SP-CSAs have a smaller defect size and larger defect density than Ni. This is attributed to the lower dislocation mobility induced by the lattice distortion of SP-CSAs. Therefore, the lattice distortion is probably the most essential characteristic which can affect the irradiation responses of SP-CSAs and defect behavior at room temperature. However, the correlation between lattice distortion and irradiation responses of SP-CSAs is still unclear.

B. Irradiation responses of SP-CSAs at high temperatures

Generally, the structural materials used in nuclear reactors are exposed to energetic particle irradiation at elevated temperatures and core structural materials to be used in proposed future advanced nuclear reactors will be exposed to higher irradiation doses and temperatures than that in current nuclear reactors.^{1,2} Therefore, the irradiation responses of SP-CSAs at high temperatures are

crucial for their applications as nuclear materials. At high temperatures, the phase stability, physicochemical/thermodynamic properties, and defect dynamics will influence the irradiation responses of SP-CSAs, thereby making the irradiation effects complicated.

1. Phase stability

Although it was originally suggested that the compositional homogeneity of HEAs is stabilized by the high configurational entropy, the effects of mixing enthalpy, which provides the thermodynamic driving force of phase separation, cannot be neglected.³³ Elements with very negative mixing enthalpy can precipitate in some extreme environments. He et al. studied the phase stability and defect cluster formation in CoCrFeNi-based SP-CSAs due to 1250 keV electron irradiation at 400 °C up to 1 dpa.³⁴ It was found that CoCrFeNi exhibits no detectable phase separation/decomposition. By contrast, FeCoCrMnNi and FeCoCrNiPd show L1₀ (NiMn)-type ordering decomposition and (001)-oriented spinodal decomposition between Co/Ni and Pd, respectively (as shown in Fig. S1). The electron irradiation-induced precipitation in both alloys is governed by the enthalpy

of mixing. However, it should be noted that no phase separation/decomposition was observed in the FeCoCrMnNi irradiated with 3 MeV Ni at 500 °C to 55 dpa.³⁵ This suggests that the phase stability of SP-CSAs under high temperature irradiation is determined not only by intrinsic thermodynamic properties but also by the irradiation conditions such as primary knock-on atom energy (potential ballistic dissolution effects) and dose rate.

A recent study on phase stability in irradiated Fe–Ni alloys concluded that the heat of mixing and the dispersion in defect migration energies were two important factors, with irradiation resistance improving with increased mixing energy and increased breadth of defect migration energies.³⁶

2. Void swelling

At typical temperatures between 0.3 and 0.6 T_M (T_M = absolute melting temperature), the agglomeration of irradiation-induced vacancies and the growth of voids can cause pronounced volume swelling, especially for pure metals and important alloys such as austenitic stainless steels, which degrades material performance and reduces its useful lifetime. Therefore, resistance to void swelling under high temperature irradiation is an important requirement for advanced nuclear reactor structural materials.

To investigate the mechanisms influencing the void swelling resistance of SP-CSAs, pure nickel and several SP-CSAs with different compositional complexities and compositions, including NiCo, NiFe, NiCoFe, NiCoFeCr, and NiCoFeCrMn, were irradiated with 1.5 MeV Ni ($3 \times 10^{15} \text{ cm}^{-2}$) and/or 3 MeV Ni ($5 \times 10^{16} \text{ cm}^{-2}$) at 500 °C.²² For the irradiation of 3 MeV Ni, TEM characterizations [as shown in Fig. 3(c)] reveal that the void swelling of SP-CSAs is significantly lower than Ni. In the irradiation of 1.5 MeV Ni at 500 °C ($3 \times 10^{15} \text{ cm}^{-2}$), the void swelling of Ni is ~1.8% while the quinary NiCoFeCrMn exhibits substantially lower void swelling ~0.02%. Based on the TEM observations, the void swelling resistance of these six materials can be ranked in the order as Ni < NiCo < NiFe ≤ NiCoFeCr < NiCoFe ≤ NiCoFeCrMn. MD simulations suggest that the different resistance to void swelling might be attributed to the different migration behavior of defect clusters. Interstitial clusters migrate randomly in 3D in NiFe but exhibit 1D migration in Ni (as shown in Fig. 4). As a consequence, interstitial clusters in Ni can migrate a long distance without encountering and annihilating vacancies. Therefore, interstitial defects in Ni can migrate from the high dpa region to the surface and to deeper regions, resulting in a high concentration of vacancies and the formation of voids in the high dpa region. By contrast, single interstitials and interstitial clusters

migrate randomly in 3D in NiFe, producing relatively high amounts of annihilation with neighboring mono-vacancies and vacancy clusters. Therefore, the concentration of voids is much smaller in NiFe. The different defect cluster migration behavior was also observed in the in situ ion irradiation.²²

The irradiation-induced void swelling in Ni and Ni-containing equiatomic alloys was also directly measured by using an optical profilometer.³⁷ Ni and six Ni-containing equiatomic alloys with face-centered cubic structure, including NiCo, NiFe, NiCoCr, NiCoFe, NiCoFeCr, and NiCoFeCrMn, were irradiated with 3 MeV Ni ions to $5 \times 10^{16} \text{ cm}^{-2}$ (peak dose ~53 dpa) at 500 °C. The samples are masked by TEM grids during ion irradiation so that irradiation-induced volume swelling could be determined by comparison. Optical profilometer measurements reveal that the six Ni-based SP-CSAs exhibit significantly lower void swelling than Ni [as shown in Fig. 3(a)]. The measured void swelling of Ni is ~6.7%, while the NiCoFeCrMn and NiCoFe show the lowest void swelling, which is <0.2% [as shown in Fig. 3(b)]. By comparison of the void swelling in various SP-CSAs, it is found that Fe is more effective in restraining the void swelling than the addition of Co.

From the above results, it can be found that SP-CSAs exhibit better resistance to void swelling than Ni under high temperature irradiation. Based on the defect distribution and MD simulation, it can be concluded that the defect migration, including the migration pathway and mobility, can be tailored in SP-CSAs. However, TEM characterizations and direct measurements show that the void swelling is not simply related with the amount of constituent elements.³⁸ For example, NiFe shows lower void swelling than NiCoCr and NiCo, and the ternary NiCoFe exhibits similar void swelling with quinary NiCoFeCrMn.³⁷ This suggests that the intrinsic properties of alloying elements should also be considered in searching for new SP-CSAs with higher irradiation tolerance.^{37,39,40}

3. Irradiation-induced defects and segregation/precipitation

Similar to the damage accumulation at room temperature, SP-CSAs also exhibit characteristic defects and defect evolutions under high temperature irradiations. The investigations on the high temperature irradiation-induced defects and their evolutions with composition, temperature, and fluence are crucial for understanding the defect behavior and estimating the material performances in real reactor environments.

Kumar et al. studied the irradiation-induced structural damage in a Co-free SP-CSA FeNiMnCr [27% Fe–28% Ni–27% Mn–18% Cr (wt%)] at temperatures ranging from room temperature to 700 °C.⁴¹ Grazing incidence

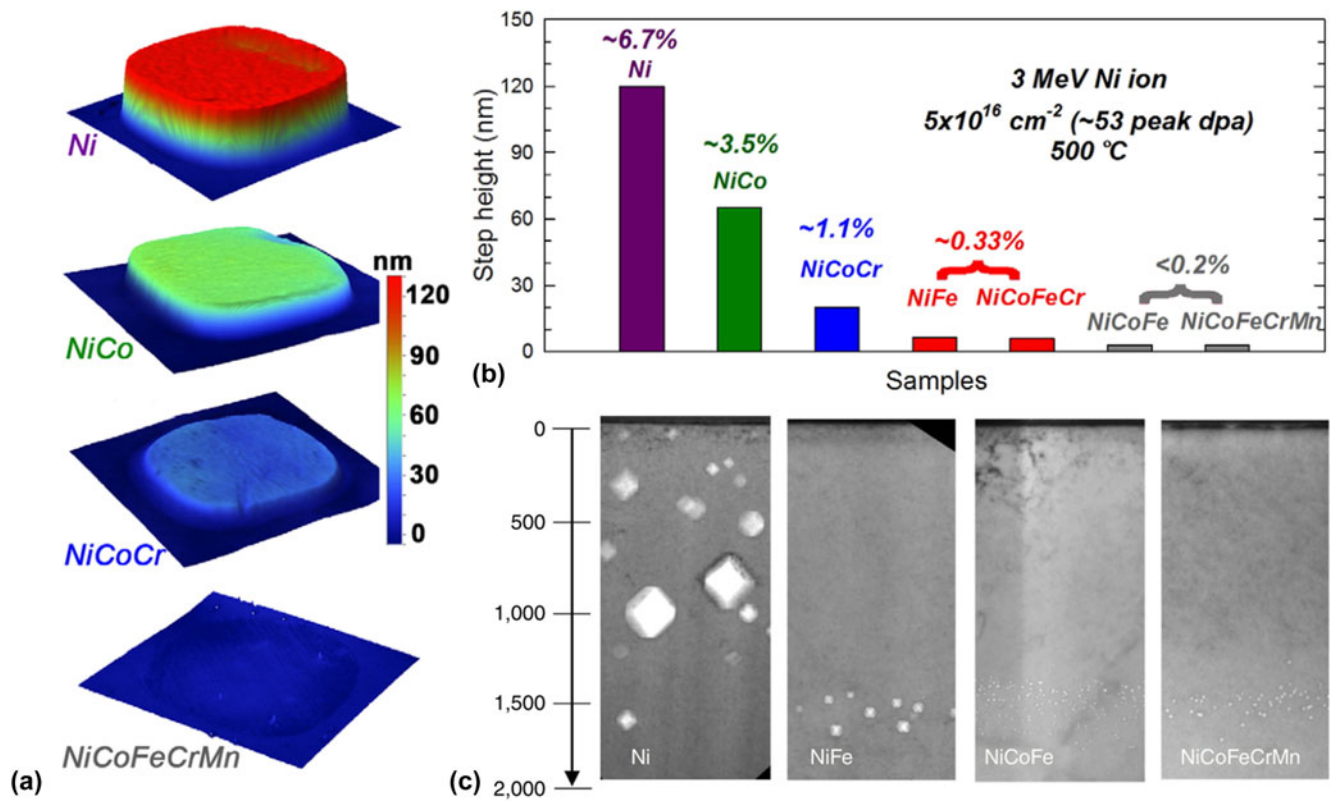


FIG. 3. Irradiation-induced volume swelling in Ni-containing equiatomic alloys irradiated with 3 MeV Ni to $5 \times 10^{16} \text{ cm}^{-2}$ at 500 °C, including (a) optical profilometer measurements of the surface swelling³⁷ (reprinted with permission from Ref. 37); (b) comparison of step-height and overall swelling of Ni and six Ni-containing equiatomic alloys³⁷ (reprinted with permission from Ref. 37); (c) cross-sectional TEM images.²² (reprinted with permission from Ref. 22).

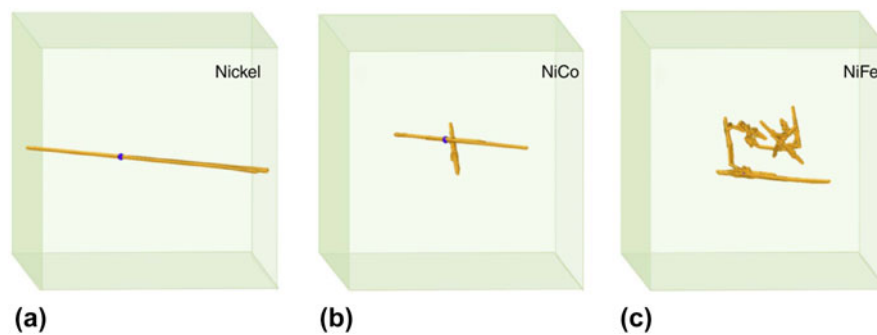


FIG. 4. MD simulation results of defect migration in (a) Ni at 800 K, (b) NiCo at 1200 K, and (c) NiFe at 1200 K.²² (reprinted with permission from Ref. 22).

X-ray diffraction revealed that single fcc phase was stable; no phase transformation or decomposition occurred in the ion irradiated samples subjected to doses up to 10 dpa and temperatures between room temperature and 700 °C. TEM characterization showed that the sizes of dislocation loops range from 1 to 10 nm in the samples irradiated at 400–700 °C. As irradiation temperature increased, only a modest increase in average dislocation loop size is found. Compared with other conventional alloys, such as Fe–Cr–Ni alloys or conventional

316 stainless steel, the variations of dislocation size and density with irradiation temperature are less pronounced for SP-CSA FeNiMnCr (as shown in Fig. 5), which are attributed to relatively sluggish solute diffusion. EDX measurements revealed that the grain boundaries were enriched with Ni, while Fe, Cr, and Mn were depleted at the grain boundaries (as shown in Supplementary Material Fig. S2). The concentration variations between matrix and grain boundary can be ranked in the order $\text{Ni} > \text{Fe} > \text{Cr} > \text{Mn}$. The solute segregations at grain

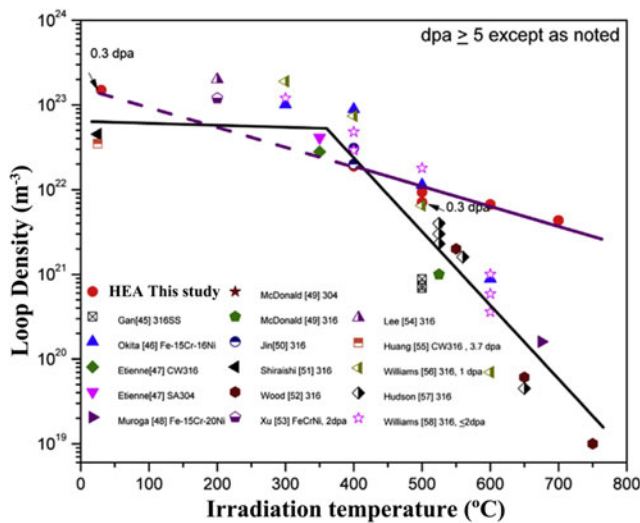


FIG. 5. Comparison of the evolution of irradiation-induced dislocation loops with temperature between FeNiMnCr HEA and other conventional alloys, including ternary Fe–Cr–Ni austenitic alloys, 316 stainless steels, and so on.⁴¹ The data sources of as-irradiated conventional alloys can be found in Ref. 41. (reprinted with permission from Ref. 41).

boundaries are significantly smaller than that of conventional Fe–20Cr–24Ni alloys.

Yang et al. compared the structural damage and chemical segregation in $\text{Al}_{0.1}\text{CoCrFeNi}$ HEAs irradiated at different temperatures ranging from 250 °C to 650 °C.⁴² Based on the TEM and APT characterizations, it is found that the $\text{Al}_{0.1}\text{CoCrFeNi}$ HEA exhibits great structural stability against high temperature irradiations; no significant phase decomposition or transformation occurs. Irradiation-induced defects include dislocation loops, network dislocations, and stacking fault tetrahedras (SFTs); defect density decreased but defect size increased with increasing irradiation temperature (as shown in Fig. 6). Furthermore, APT characterization quantitatively measured the ion irradiation induced-enrichment of Ni and Co as well as the depletion of Fe and Cr at defect clusters, mainly including dislocation loops and dislocations, and its evolution with irradiation temperature (as shown in Fig. 6). The concentrations of Co, Cr, Fe, and Ni vary by 30–50% between the matrix and dislocation loops and the concentration fluctuation at 250 °C is smaller than that of other three temperatures. Co and Fe show slightly more segregation than the Ni and Cr, respectively.

The irradiation-induced structural damage and segregations at 500 °C were recently compared in NiFe, NiCoFe, NiCoFeCr, and NiCoFeCrMn.³⁵ The four SP-CSAs were irradiated with 3 MeV Ni at 500 °C to $5 \times 10^{16} \text{ cm}^{-2}$. TEM characterizations revealed that irradiation-induced dislocation loops include perfect loops with $\mathbf{b} = \langle 110 \rangle / 2$ and Frank loops with $\mathbf{b} = \langle 111 \rangle / 3$ (as shown in Fig. 7), which is similar with

the high energy electron irradiation.^{34,43} The binary NiFe exhibits the largest loop size and lowest loop density, while NiCoFeCrMn presents the smallest loop size and lowest loop density. However, the ternary NiCoFe and quaternary NiCoFeCr exhibit comparable loop density and loop size. Only the fraction of Frank loops clearly increases with increasing composition complexity. Irradiation-induced segregation at Frank loops was measured using electron energy loss spectroscopy. It was found that Frank dislocation loops are enriched with Ni and Co, and depleted with Cr and Fe in NiFe, NiCoFe, and NiCoFeCr. No obvious segregation is detected in as-irradiated quinary NiCoFeCrMn, indicating that the irradiation-induced segregation is significantly lower in NiCoFeCrMn than in other three SP-CSAs. Furthermore, NiCoFeCr exhibits a slightly lower segregation than NiFe and NiCoFe. The evolutions of irradiation-induced defects and segregations in the four SP-CSAs clearly indicate that alloy composition plays a significant role in the irradiation responses of SP-CSAs. The authors propose that the high lattice distortion in complex alloys can decrease the mobility of interstitial defects, therefore, restraining the evolutions of dislocation loops and irradiation-induced segregation.

The experiment results summarized above show the effects of composition complexity on the behavior of interstitial defects are similar with that of vacancy-type defects, the migration behavior of both types of defects can be tailored, restraining or delaying the defect evolutions, including defect incubation and growth. Furthermore, irradiation-induced segregation at grain boundaries and defect clusters is also decreased in complex SP-CSAs, suggesting the probable good resistance to irradiation-assisted stress corrosion cracking.

III. MODELING STUDIES OF DEFECT BEHAVIOR IN SP-CSAs

The process of irradiation damage covers a wide range of time and length scales. Irradiation damage is initiated by collisions of energetic neutrons with lattice atoms, resulting in displacement cascades and supersaturation of vacancies and self-interstitials in a much localized region. The characteristic length of displacement cascade is $\sim 10 \text{ nm}$, and the cascade event only lasts for 1–100 picoseconds. On the other hand, the microstructure and mechanical properties of the irradiated material are not only dependent upon displacement cascade but also on the long-range and long-term diffusion and reaction of irradiation-produced defects.⁴ Thus, a hierarchical multi-scale modeling approach^{44–46} has been developed to simulate irradiation effects over all related length and time scale, as shown in Supplementary Material Fig. S3. At the very fundamental level, ab initio electronic structure modeling is used to obtain basic defect

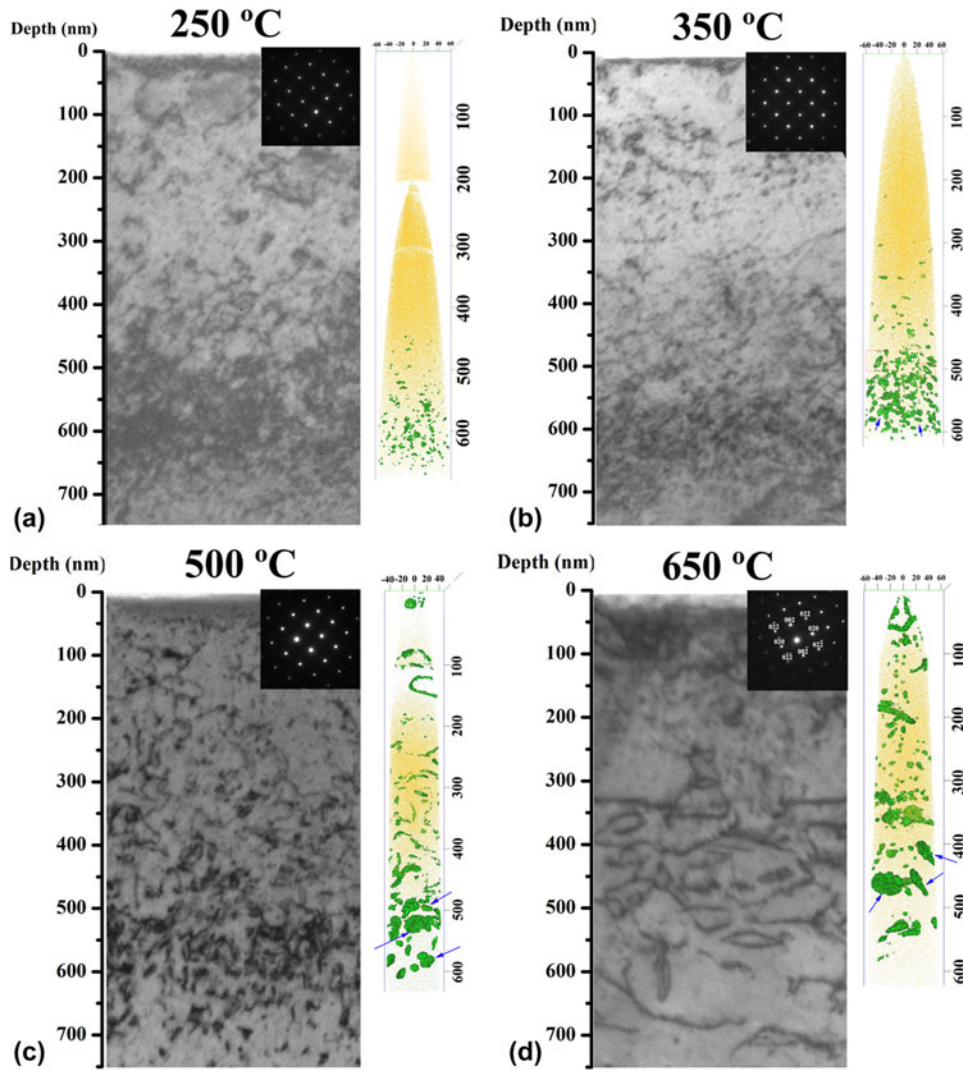


FIG. 6. Cross-sectional TEM images and corresponding SAED patterns of $\text{Al}_{0.1}\text{CoCrFeNi}$ irradiated with 3 MeV Au to $6 \times 10^{15} \text{ cm}^{-2}$ at (a) 250 °C; (b) 350 °C; (c) 500 °C; and (d) 650 °C, respectively. APT results of 55 at.% Ni + Co iso-concentration surfaces of $\text{Al}_{0.1}\text{CoCrFeNi}$ irradiated at the four different temperatures are also given. The deposited Au ions are marked by background contrast. The disk-shaped and ring-shaped dislocation loops are marked by arrows and rectangles, respectively.⁴² (reprinted with permission from Ref. 42).

properties, such as point defect formation and migration energies. While MD simulation can track the evolution of displacement cascade and also provide insights on defect kinetics and interaction mechanisms. The long-range and long-term effects, on the other hand, can be modeled by the kinetic Monte Carlo (KMC) method^{47,48} by utilizing the displacement cascade database from MD and defect properties from ab initio modeling.

In Sec. III.A and III.B, theoretical calculations and simulation work on SP-CSAs will be reviewed. Since the research of irradiation effects in SP-CSAs is in a nascent stage, most of the current studies are focused on ab initio calculation of defect energetics and MD modeling of primary irradiation damage stage, such as displacement cascade evolution and short-range transport of defects.

A. Ab initio study of defect energetics

Due to the complex nature of many-body interactions, only several semi-empirical potentials have been developed for two- or three-component systems and basically none for four or more component systems. Thus, ab initio defect energetics will not only facilitate the understanding of defect physics in SP-CSAs but also provide a robust database to develop and validate semi-empirical potentials for MD modeling of concentrated, multicomponent systems. Reliable implementation of ab initio and MD modeling will then establish the foundation for upper-hierarchy KMC modeling and eventually reveal the evolution of microstructures over long times and large length scales. It should be noted that some common concepts in modeling pure metals and dilute

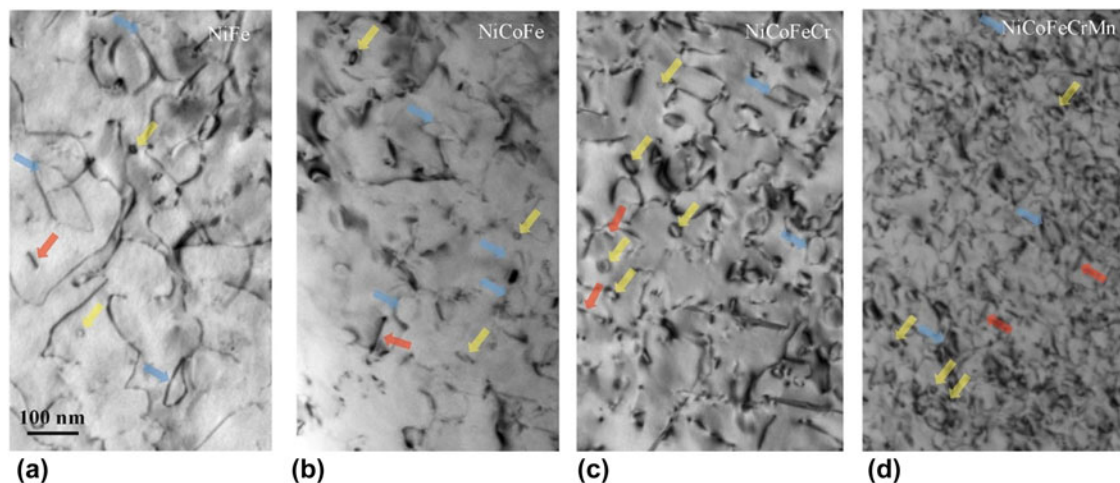


FIG. 7. BF TEM images of (a) NiFe; (b) NiCoFe; (c) NiCoFeCr; and (d) NiCoFeCrMn irradiated with 3 MeV Ni up to 38 ± 5 dpa at 500 °C.³⁵ (reprinted with permission from Ref. 35).

alloys cannot be applied for SP-CSAs. Generally, point defects just have one or several formations and migration energies in pure metals and dilute alloys. However, the energetics of point defects can no longer be evaluated as some discrete values but instead require treatment as statistical distributions in SP-CSAs due to the vast possibilities of local chemical surroundings near defects induced by compositional complexity. Therefore, the defect energetics, such as defect formation energies and migration barriers, exhibit statistical distributions in SP-CSAs. To understand defect behavior in SP-CSAs, it is important to characterize these distributions.

Point defect formation energies determine the equilibrium concentrations of vacancies and interstitials at a given temperature. Based on density functional theory (DFT) and empirical potentials, the distributions of defect energetics in several Ni-based SP-CSAs have been studied and their specific features are revealed.^{49,50} In general, it is found that in Ni-based binary SP-CSAs, the formation energies of interstitial dumbbells are lower than those in pure Ni (~ 4.27 eV), whereas the formation energies of vacancies are higher (~ 1.47 eV for Ni), as shown in Figs. 8(a) and 8(b). In addition, preferable binding is observed as some interstitial dumbbells exhibit lower formation energies than others. For example, Ni-contained dumbbells show lower formation energies than Fe-contained in NiFe. Compared with these binary systems, the statistical spread of vacancy and interstitial formation energies in NiCoCr and NiCoCrFe are generally larger.^{50–52} However, studies based on smaller supercells (20–30 atoms)^{51,52} produce wider spread statistical spread of formation energies than that based on large supercells (more than 100 atoms).⁵⁰

In addition to supercell size effects, different chemical potentials used in these studies can also contribute to the discrepancies in the statistical spread. Chen et al.,⁵¹

Middleburgh et al.,⁵² and Zhao et al.⁵⁰ studied the vacancy formation energy in the NiCoCrFe SP-CSA system. Chen et al.⁵¹ and Middleburgh et al.⁵² used 20–30 atom supercells and used pure metal as the reference chemical potential, while Zhao et al.⁵⁰ used a 256-atom supercell and directly compute chemical potentials in NiCoCrFe environment, which takes longer computational time but is a more reasonable representation for the SP-CSA by greatly reducing the periodic image effect and accounting for the effect of chemical disorder on chemical potential. Vacancy formation energy ranges from 0.7 to 3.1 eV and -0.75 to 2.75 eV in the calculation results of Chen et al.⁵¹ and Middleburgh et al.,⁵² respectively. By contrast, Zhao et al.⁵⁰ calculation results show a much smaller distribution of the formation energy of vacancy, which is 1.55–2.25 eV. Since the formation energies of point defect and defect cluster are important for the development and testing of semi-empirical potentials for studying irradiation effects (displacement cascade evolution, defect cluster interactions) by MD simulation in SP-CSAs, it is critical to carefully evaluate the trade-off between computation cost and computational setup (i.e., supercell size and chemical potentials).

The distributions of defect migration energies in several Ni-based SP-CSAs have also been studied and their specific features are revealed.^{49,50} As compared with Ni, larger barriers are found for interstitials in both NiCoCr and NiCoFeNi, whereas lower barriers are observed for vacancies.⁵⁰ These results suggest that in SP-CSAs, the interstitial diffusion becomes slower whereas vacancy diffusion becomes faster, which may enhance the interaction between interstitials and vacancies and contribute to enhanced defect recombination. In particular, an increasing overlap region between the distributions of migration energies for interstitials and

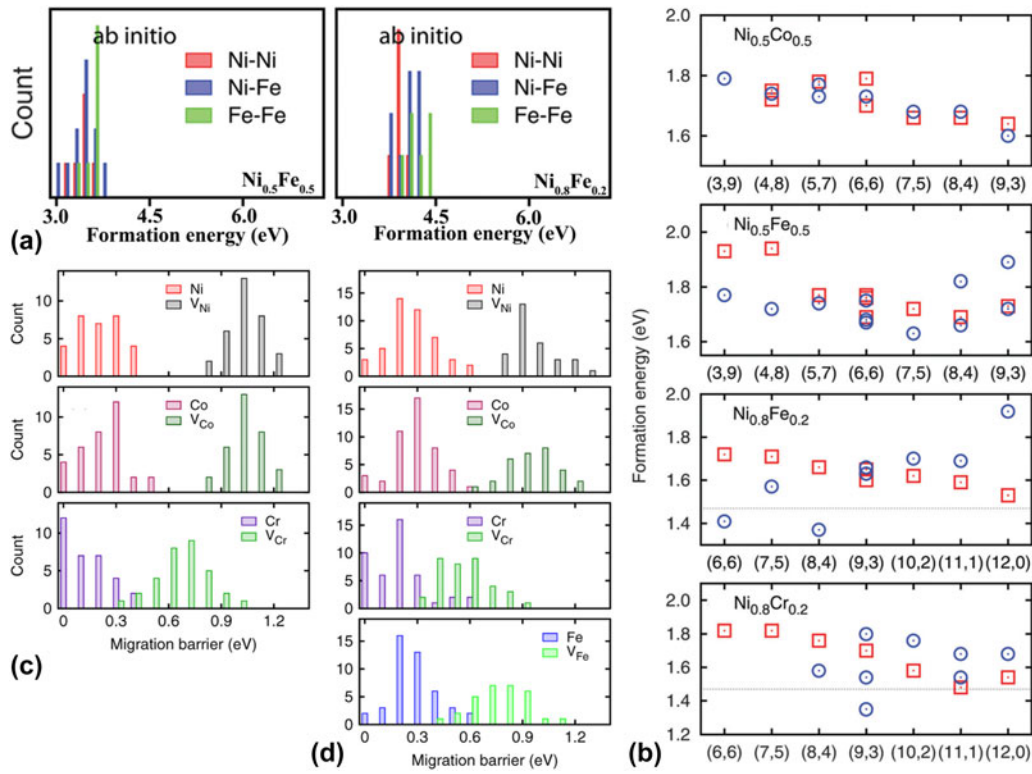


FIG. 8. Ab initio calculation results: (a) Formation energies of a [100] dumbbell in $\text{Ni}_{0.5}\text{Fe}_{0.5}$ (left column) and $\text{Ni}_{0.8}\text{Fe}_{0.2}$ (right column); (b) Formation energies of vacancy in four Ni-based binary SP-CSAs as a function of the number of its nearest neighbor pair (m, n), where m is the number of Ni and n is the number of Fe or Cr⁴⁹ (reprinted with permission from Ref. 49). Migration barriers of interstitials and vacancies in (c) NiCoCr and (d) NiCoFeCr.⁵⁰ (reprinted with permission from Ref. 50).

vacancies is found from binary NiFe, to ternary NiCoCr and quaternary NiCoFeCr [as shown in Figs. 8(c) and 8(d)].^{49,50} The increasing overlap region suggests that defect recombination and annihilation may be greatly facilitated in these SP-CSAs. On the other hand, these ab initio studies of migration barriers show that both vacancies and interstitials have a huge variety of migration pathways to choose from depending on the chemical environment of defects. This finding was also recently illustrated through a larger vacancy migration energy statistics of NiFe SP-CSAs based on semi-empirical potentials.³⁶ The fluctuation in point defect migration barriers over the potential energy landscape of SP-CSAs shows that the defect transport in SP-CSAs is spatially heterogeneous and directionally anisotropic. Both of these two effects can have strong implications on the possible sluggish diffusion kinetics of SP-CSA.

B. MD simulation: displacement cascade evolution and defect dynamics

MD simulations based on either DFT (ab initio MD, AIMD) or empirical potentials (CMD: classical MD) have been used to study the evolution and diffusion of defect and defect clusters in SP-CSAs. MD simulations

on several Ni-based SP-CSAs have revealed that self-interstitials form dislocation loops on [111] planes with $1/3\langle 111 \rangle$ Burgers vector and vacancies tend to form SFTs^{29,53,54}; both are in consistent with experimental observation of the alloys irradiated by 3 MeV Au ions at room temperature. Compared with pure Ni, NiFe, and NiCr alloys show slower loop formation kinetics, resulting in a smaller loop size. The surviving defects in Ni-Fe and Ni-Cr binaries are composition dependent. On the other hand, the simulations at high temperature show that Cr leads to faster SFT formation in Ni-Cr binary and ternary SP-CSAs with large Cr content.

A more detailed MD study was conducted by Zhang et al.²¹ to compare displacement cascade evolution between Ni and NiFe. Similarly, MD results show that vacancies form SFTs and interstitials form small dislocation loops of $1/3\langle 111 \rangle[111]$ type and $1/2\langle 110 \rangle[110]$ type in NiFe. In addition, the number of surviving stable defects after displacement cascade is higher in Ni than in NiFe by a factor of 2, which is qualitatively consistent with results from experiment. Defect configuration and reduction in damage are also reported in similar MD study conducted by Béland et al.⁵⁵ In addition to the Ni-Fe system, reduction in damage is also found in the NiCo system compared with pure Ni. Béland et al.⁵⁶

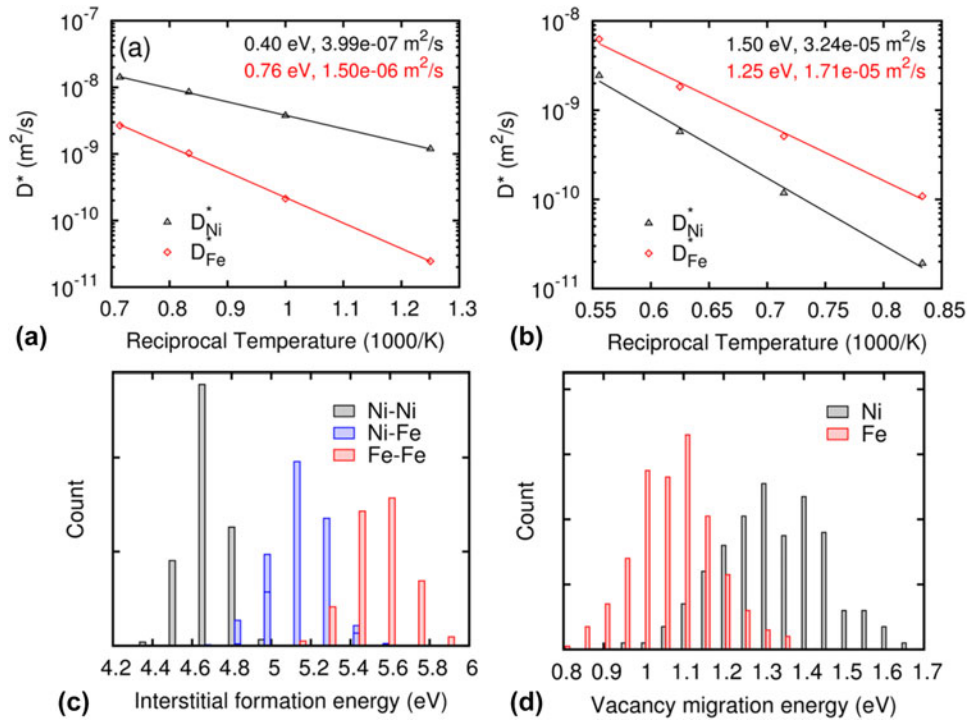


FIG. 9. Tracer diffusion coefficients due to (a) interstitial atom and (b) vacancy diffusion in NiFe; (c) the formation energies of interstitial dumbbells and (d) vacancy migration energy.⁶⁰ (reprinted with permission from Ref. 60).

also showed that the difference in the production of large defects between Ni and NiFe is not related to the ballistic of collision cascade. Koch et al.⁵⁷ studied a chemically more complex SP-CSA, CuNiCoFe. In addition to the point defect and defect clusters produced by the displacement cascade, this study also investigates the change in the chemical disorder after irradiation and concludes that compared with de-mixing effects, irradiation drives the alloy toward random solid solution. Since an increase in chemical disordering is believed to prohibit the growth of defect clusters, the effect of irradiation mixing in SP-CSA can also contribute to the reduced damage accumulation observed in ion irradiation experiments.

MD studies can also provide insight on diffusion of defect and defect clusters in SP-CSAs.^{22,58–60} For point defect diffusion, both AIMD and CMD show that both interstitials and vacancies are diffusing more sluggish in NiFe than in pure Ni. Furthermore, there is chemically biased diffusion in SP-CSAs. Specifically, the diffusion of one component is faster than others in SP-CSAs. For example, in NiFe, it is shown that interstitial diffusion is dominated by the Ni sublattice whereas vacancy diffusion occurs mainly through the Fe sublattice. As a result, the tracer diffusion coefficient of Ni is higher than that of Fe in the case of interstitial diffusion, whereas Fe is higher in case of vacancy diffusion, as shown by the calculated partial diffusion coefficients in Figs. 9(a) and 9(b). The

reason for this observation can be traced back to their different defect energies. For interstitial diffusion, the interstitial atom prefers to jump to Ni sublattice because of the lower formation energies of Ni-contained dumbbells, as displayed in Fig. 9(c). The diffusion of vacancy, on the other hand, depends on vacancy migration energies. As migration barriers of Fe vacancy are lower than those of Ni [as shown in Fig. 9(d)], vacancy migrates through exchange among the Fe sublattice. Note that these results are obtained using the Bonny 2011 potential,⁶¹ which has been proved to yield similar defect energies to ab initio calculations.⁴⁹ In fact, such preferable interstitial binding and vacancy migration are also found in ternary and quaternary SP-CSAs by ab initio calculations.⁵⁰

For defect cluster diffusions, CMD simulations show that large vacancy clusters tend to become slower in CSAs, which help to suppress the vacancy cluster growth in SP-CSAs. CMD results show that intestinal cluster diffusion proceeds through 3-dimensional motion, in contrast to 1-dimensional motion in pure Ni, which helps to decrease the void swelling in SP-CSAs, as discussed in Sec. II.B.2 and Fig. 4. The motion of dislocation is also studied by CMD, which demonstrates that dislocation movement is slower in SP-CSAs.⁶² This result, combined with the suppressed growth of vacancy clusters, is responsible for the delayed damage accumulation found in SP-CSAs.⁶³

IV. PERSPECTIVES

Due to increasing interest in the irradiation tolerance of SP-CSAs, improved fundamental understanding of irradiation effects of SP-CSAs is being acquired, including the accumulation of structural damage, void swelling, phase stability, and solute segregation. However, several scientific challenges should be considered and solved for the further application of SP-CSAs in advanced nuclear reactors.

First, most of these studies are focused on several model SP-CSAs, such as NiCo, NiFe, NiCoFeCr, NiCoFe, and NiCoFeCrMn, which contain high concentrations of Ni and/or Co that exhibit high induced radioactivity under neutron irradiation. High neutron activation elements should be avoided in nuclear reactor materials to reduce radioactivity for maintenance or waste disposal. For example, fusion material scientists have developed reduced-activation ferritic–martensitic steel, in which the typical long-decay-producing alloy elements Mo, Nb, Ni, Cu, and N are minimized or replaced by other low activation elements, such as W, V, and Ta.⁶⁴ Therefore, it is important to design SP-CSAs with low neutron activation. However, it should be noted that the formation of SP-CSAs is limited to a small number of elements and the alloy compositions should satisfy several thermodynamic rules and requirements so that to date, only a limited number of SP-CSA compositions have been identified.³³

Second, most current experiment results are focused on the comparison of irradiation tolerances of SP-CSAs with different numbers of principal components to investigate the effects of compositional complexity on the irradiation resistance. However, it has been found that the properties of SP-CSAs, including mechanical properties and irradiation tolerance, are nonmonotonically dependent on compositional complexity. For example, the strength, ductility, and toughness of the ternary SP-CSA CrCoNi exceed the properties of all other SP-CSAs reported to date.⁹ Furthermore, NiFe shows lower void swelling than NiCoCr and NiCo, and the ternary NiCoFe exhibits similar void swelling with quinary NiCoFeCrMn under an ion irradiation of 3 MeV Ni at 500 °C.³⁷ These results demonstrate that compositional complexity is not the only factor which can influence the irradiation tolerance of SP-CSAs; additional factors such as lattice distortion, specific alloying elements, and corresponding concentrations also need to be considered to reveal fundamental mechanisms determining the defect behavior and irradiation tolerance of SP-CSAs. In addition, the accumulation of irradiation-induced structural damage near room temperature is suppressed in SP-CSAs at low fluence, but several SP-CSAs exhibit higher saturation damage than Ni at high fluence.⁶⁵ This indicates that the defect evolutions with fluence are different in various SP-CSAs,

suggesting that complicated defect accumulation behavior may occur in various SP-CSAs.

Third, the concept of SP-CSAs originates from HEAs. HEAs contain at least four principal components, while SP-CSAs only require ≥ 2 principal components. Both HEAs and SP-CSAs are single phase and most of the alloys investigated to date are single fcc phase. In the investigations of HEAs, a great number of multicomponent concentrated alloys are explored, but most of them are multiphase. However, many of the multiphase concentrated alloys have various good mechanical properties,^{66–71} such as good high temperature mechanical properties due to the formation of numerous precipitates (precipitate-strengthened). Furthermore, the numerous precipitates introduce high density interfaces, which can act as sinks for the recombination of irradiation-induced defects, enhancing the irradiation resistance. Since the multiphase concentrated alloys are not limited by the single phase structure, the number of multiphase concentrated alloys is much more than SP-CSAs, which provides more choices in the composition, microstructure, and mechanical property. Based on these characteristics, the multiphase concentrated alloys have more remarkable potential for use as structural materials in the advanced nuclear reactors. However, the microstructures of multiphase concentrated alloys are more complicated than SP-CSAs, requiring additional careful and comprehensive characterization work.

Finally, nearly all of the irradiation studies performed to date on HEAs and SP-CSAs are limited to single ion beams. Additional research is needed to examine the effect of He (produced from neutron transmutations) on microstructural evolution of SP-CSAs during high dose irradiation, along with investigations of dose rate effects and more comprehensive studies performed over a broad range of temperatures.

As for theoretical modeling, more detailed *ab initio* and MD simulation of defect properties are needed to understand irradiation effects in SP-CSAs. Modeling work so far has shown that chemical disorder can alter both the thermodynamics and kinetics of defect and defect clusters, but most of the findings are restricted for binary systems, which have similar degree of chemical disorder as conventional concentrated Fe–Ni–Cr alloys. Other than several preliminary studies,^{50–52} the effects of chemical disorder as well as unique effects of certain chemical species on defect energetics in ternary, quaternary, and five-component systems are still largely an unexplored regime. Besides, many current MD studies show qualitative agreement with experimental characterization results of ion irradiated SP-CSAs. To obtain models with better interpretive and even predictive ability of experimental phenomena, more effort is needed to refine the methods and physics behind the models to reach quantitative agreement. To accomplish that,

advanced multibody semi-empirical potentials, based on larger ab initio defect energy database and state-of-art potential fitting strategy, need to be developed as the foundation to not only capture the right physics during displacement cascade evolution, defect migration, and defect interaction but also obtain better quantitative accuracy of defect cluster size and density distribution.

V. CONCLUSIONS

The present paper summarizes the recent progress in the irradiation responses and defect behavior of SP-CSAs and HEAs, including the (i) accumulation of irradiation-induced structural damage at room temperature; (ii) phase stability, void swelling resistance, segregation behavior, and defect evolution of SP-CSAs irradiated at high temperatures; (iii) defect behavior of SP-CSAs derived from ab initio and MD studies. Generally, SP-CSAs exhibit a better irradiation tolerance than pure Ni, including slower accumulation of irradiation-induced structural damage (in low fluence range) and lower void swelling. Furthermore, no significant phase decomposition or transformation occurs under irradiation, suggesting a good phase stability of SP-CSAs under irradiation. However, the irradiation responses of SP-CSAs show a nonmonotonic variation with compositional complexity (number of principal elements), which indicates both the compositional complexity and alloying elements contribute to the irradiation responses of SP-CSAs. This makes the irradiation responses of SP-CSAs can be tailored in a wide range by compositional complexity and alloying elements, which enhances the flexibility of SP-CSAs for using in advanced nuclear energy systems.

Although significant progress has been made in the irradiation responses and defect behavior of SP-CSAs, several scientific challenges still exist in the applications of SP-CSAs in the advanced nuclear system, such as high neutron activation in many of the alloys, and the chemical effects of alloying elements. However, the fascinating properties of SP-CSAs and their great potential to be used in advanced nuclear energy systems motivate more comprehensive research studies to obtain a deeper understanding of the defect behavior in SP-CSAs and design SP-CSAs with higher performances for nuclear applications.

ACKNOWLEDGMENTS

TY, CY, and SJZ were supported by the Office of Fusion Energy, U.S. Department of Energy (Grant No. DE-SC0006661 with the University of Tennessee). YZ, SZ, and HB were supported as part of the Energy Dissipation to Defect Evolution (EDDE), an Energy Frontier Research Center funded by the U.S. Department of Energy, Office of Science, Basic Energy Sciences.

REFERENCES

1. S. Chu and A. Majumdar: Opportunities and challenges for a sustainable energy future. *Nature* **488**, 294 (2012).
2. Y. Guérin, G.S. Was, and S.J. Zinkle: Materials challenges for advanced nuclear energy systems. *MRS Bull.* **34**, 10 (2009).
3. S.J. Zinkle and G. Was: Materials challenges in nuclear energy. *Acta Mater.* **61**, 735 (2013).
4. G. Odette, M. Alinger, and B. Wirth: Recent developments in irradiation-resistant steels. *Annu. Rev. Mater. Res.* **38**, 471 (2008).
5. T. Allen, H. Burlet, R.K. Nanstad, M. Samaras, and S. Ukai: Advanced structural materials and cladding. *MRS Bull.* **34**, 20 (2009).
6. S.J. Zinkle and L.L. Snead: Designing radiation resistance in materials for fusion energy. *Annu. Rev. Mater. Res.* **44**, 241 (2014).
7. P. Yvon: *Structural Materials for Generation IV Nuclear Reactors* (Woodhead Publishing, Kidlington, U.K., 2016); pp. 569–586.
8. B. Gludovatz, A. Hohenwarter, D. Catoor, E.H. Chang, E.P. George, and R.O. Ritchie: A fracture-resistant high-entropy alloy for cryogenic applications. *Science* **345**, 1153 (2014).
9. B. Gludovatz, A. Hohenwarter, K.V. Thurston, H. Bei, Z. Wu, E.P. George, and R.O. Ritchie: Exceptional damage-tolerance of a medium-entropy alloy CrCoNi at cryogenic temperatures. *Nat. Commun.* **7**, 10602 (2016).
10. F. Otto, A. Dlouhý, C. Somsen, H. Bei, G. Eggeler, and E.P. George: The influences of temperature and microstructure on the tensile properties of a CoCrFeMnNi high-entropy alloy. *Acta Mater.* **61**, 5743 (2013).
11. M.A. Hemphill, T. Yuan, G.Y. Wang, J.W. Yeh, C.W. Tsai, A. Chuang, and P.K. Liaw: Fatigue behavior of Al_{0.5}CoCrCuFeNi high entropy alloys. *Acta Mater.* **60**, 5723 (2012).
12. C.-Y. Hsu, J.-W. Yeh, S.-K. Chen, and T.-T. Shun: Wear resistance and high-temperature compression strength of Fcc CuCoNiCrAl_{0.5}Fe alloy with boron addition. *Metall. Mater. Trans. A* **35**, 1465 (2004).
13. P.K. Huang, J.W. Yeh, T.T. Shun, and S.K. Chen: Multi-principal-element alloys with improved oxidation and wear resistance for thermal spray coating. *Adv. Eng. Mater.* **6**, 74 (2004).
14. Y.J. Zhou, Y. Zhang, Y.L. Wang, and G.L. Chen: Solid solution alloys of AlCoCrFeNiTi_x with excellent room-temperature mechanical properties. *Appl. Phys. Lett.* **90**, 181904 (2007).
15. X.F. Wang, Y. Zhang, Y. Qiao, and G.L. Chen: Novel microstructure and properties of multicomponent CoCrCuFeNiTi_x alloys. *Intermetallics* **15**, 357 (2007).
16. Y.P. Wang, B.S. Li, M.X. Ren, C. Yang, and H.Z. Fu: Microstructure and compressive properties of AlCrFeCoNi high entropy alloy. *Mater. Sci. Eng., A* **491**, 154 (2008).
17. C.-Y. Hsu, W.-R. Wang, W.-Y. Tang, S.-K. Chen, and J.-W. Yeh: Microstructure and mechanical properties of new AlCo_xCrFeMo_{0.5}Ni high-entropy alloys. *Adv. Eng. Mater.* **12**, 44 (2010).
18. Y. Chen, U. Hong, J. Yeh, and H. Shih: Selected corrosion behaviors of a Cu_{0.5}NiAlCoCrFeSi bulk glassy alloy in 288 °C high-purity water. *Scripta Mater.* **54**, 1997 (2006).
19. W. Zhang, P.K. Liaw, and Y. Zhang: Science and technology in high-entropy alloys. *Sci. China Mater.* **61**, 2 (2018).
20. K.-Y. Tsai, M.-H. Tsai, and J.-W. Yeh: Sluggish diffusion in Co–Cr–Fe–Mn–Ni high-entropy alloys. *Acta Mater.* **61**, 4887 (2013).
21. Y. Zhang, G.M. Stocks, K. Jin, C. Lu, H. Bei, B.C. Sales, L. Wang, L.K. Béland, R.E. Stoller, G.D. Samolyuk, M. Caro, A. Caro, and W.J. Weber: Influence of chemical disorder on energy dissipation and defect evolution in concentrated solid solution alloys. *Nat. Commun.* **6**, 8736 (2015).
22. C. Lu, L. Niu, N. Chen, K. Jin, T. Yang, P. Xiu, Y. Zhang, F. Gao, H. Bei, and S. Shi: Enhancing radiation tolerance by controlling defect mobility and migration pathways in multicomponent single-phase alloys. *Nat. Commun.* **7**, 13564 (2016).

23. T. Koppelaar, W. Yeh, and R. Cotterill: Lattice defects in neutron irradiated α Cu solid solution alloys. *Philos. Mag.* **13**, 867 (1966).
24. S. Zinkle: Microstructure and properties of copper alloys following 14-MeV neutron irradiation. *J. Nucl. Mater.* **150**, 140 (1987).
25. C. English: Low-dose neutron irradiation damage in FCC and BCC metals. *J. Nucl. Mater.* **108**, 104 (1982).
26. A. Stathopoulos, C. English, B. Eyre, and P. Hirsch: The effect of alloying additions on collision cascades in heavy-ion irradiated copper solid solutions. *Philos. Mag. A* **44**, 309 (1981).
27. T. Robinson and M. Jenkins: Heavy-ion irradiation of nickel and nickel alloys. *Philos. Mag. A* **43**, 999 (1981).
28. N. Hashimoto, T. Byun, and K. Farrell: Microstructural analysis of deformation in neutron-irradiated fcc materials. *J. Nucl. Mater.* **351**, 295 (2006).
29. D.S. Aidhy, C. Lu, K. Jin, H. Bei, Y. Zhang, L. Wang, and W.J. Weber: Point defect evolution in Ni, NiFe, and NiCr alloys from atomistic simulations and irradiation experiments. *Acta Mater.* **99**, 69 (2015).
30. F. Granberg, K. Nordlund, M.W. Ullah, K. Jin, C. Lu, H. Bei, L.M. Wang, F. Djurabekova, W.J. Weber, and Y. Zhang: Mechanism of radiation damage reduction in equiatomic multicomponent single phase alloys. *Phys. Rev. Lett.* **116**, 135504 (2016).
31. K. Jin, W. Guo, C. Lu, M.W. Ullah, Y. Zhang, W.J. Weber, L. Wang, J.D. Poplawsky, and H. Bei: Effects of Fe concentration on the ion-irradiation induced defect evolution and hardening in Ni-Fe solid solution alloys. *Acta Mater.* **121**, 365 (2016).
32. C. Lu, K. Jin, L.K. Béland, F. Zhang, T. Yang, L. Qiao, Y. Zhang, H. Bei, H.M. Christen, and R.E. Stoller: Direct observation of defect range and evolution in ion-irradiated single crystalline Ni and Ni binary alloys. *Sci. Rep.* **6**, 19994 (2016).
33. F. Otto, Y. Yang, H. Bei, and E.P. George: Relative effects of enthalpy and entropy on the phase stability of equiatomic high-entropy alloys. *Acta Mater.* **61**, 2628 (2013).
34. M.-R. He, S. Wang, S. Shi, K. Jin, H. Bei, K. Yasuda, S. Matsumura, K. Higashida, and I.M. Robertson: Mechanisms of radiation-induced segregation in CrFeCoNi-based single-phase concentrated solid solution alloys. *Acta Mater.* **126**, 182 (2017).
35. C. Lu, T. Yang, K. Jin, N. Gao, P. Xiu, Y. Zhang, F. Gao, H. Bei, W.J. Weber, K. Sun, Y. Dong, and L. Wang: Radiation-induced segregation on defect clusters in single-phase concentrated solid-solution alloys. *Acta Mater.* **127**, 98 (2017).
36. M. Jin, P. Cao, and M.P. Short: Thermodynamic mixing energy and heterogeneous diffusion uncover the mechanisms of radiation damage reduction in single-phase Ni-Fe alloys. *Acta Mater.* **147**, 16 (2018).
37. K. Jin, C. Lu, L.M. Wang, J. Qu, W.J. Weber, Y. Zhang, and H. Bei: Effects of compositional complexity on the ion-irradiation induced swelling and hardening in Ni-containing equiatomic alloys. *Scripta Mater.* **119**, 65 (2016).
38. E. Levo, F. Granberg, C. Fridlund, K. Nordlund, and F. Djurabekova: Radiation damage buildup and dislocation evolution in Ni and equiatomic multicomponent Ni-based alloys. *J. Nucl. Mater.* **490**, 323 (2017).
39. Y. Zhang, S. Zhao, W.J. Weber, K. Nordlund, F. Granberg, and F. Djurabekova: Atomic-level heterogeneity and defect dynamics in concentrated solid-solution alloys. *Curr. Opin. Solid State Mater. Sci.* **21**, 221 (2017).
40. K. Jin, B.C. Sales, G.M. Stocks, G.D. Samolyuk, M. Daene, W.J. Weber, Y. Zhang, and H. Bei: Tailoring the physical properties of Ni-based single-phase equiatomic alloys by modifying the chemical complexity. *Sci. Rep.* **6**, 20159 (2016).
41. N.A.P.K. Kumar, C. Li, K.J. Leonard, H. Bei, and S.J. Zinkle: Microstructural stability and mechanical behavior of FeNiMnCr high entropy alloy under ion irradiation. *Acta Mater.* **113**, 230 (2016).
42. T. Yang, S. Xia, W. Guo, R. Hu, J.D. Poplawsky, G. Sha, Y. Fang, Z. Yan, C. Wang, and C. Li: Effects of temperature on the irradiation responses of Al_{0.1}CoCrFeNi high entropy alloy. *Scripta Mater.* **144**, 31 (2018).
43. M.-R. He, S. Wang, K. Jin, H. Bei, K. Yasuda, S. Matsumura, K. Higashida, and I.M. Robertson: Enhanced damage resistance and novel defect structure of CrFeCoNi under in situ electron irradiation. *Scripta Mater.* **125**, 5 (2016).
44. B.D. Wirth, M.J. Caturla, T. Diaz de la Rubia, T. Khraishi, and H. Zbib: Mechanical property degradation in irradiated materials: A multiscale modeling approach. *Nucl. Instrum. Methods Phys. Res., Sect. B* **180**, 23 (2001).
45. B.D. Wirth, G.R. Odette, J. Marian, L. Ventelon, J.A. Young-Vandersall, and L.A. Zepeda-Ruiz: Multiscale modeling of radiation damage in Fe-based alloys in the fusion environment. *J. Nucl. Mater.* **329–333**(Part A), 103 (2004).
46. L. Malerba, A. Caro, and J. Wallenius: Multiscale modelling of radiation damage and phase transformations: The challenge of FeCr alloys. *J. Nucl. Mater.* **382**, 112 (2008).
47. A.F. Voter: Introduction to the kinetic Monte Carlo method. In *Radiation Effects in Solids*, K.E. Sickafus, E.A. Kotomin, and B.P. Uberuaga, eds. (Springer, Dordrecht, The Netherlands, 2007); p. 1.
48. A. Chatterjee and D.G. Vlachos: An overview of spatial microscopic and accelerated kinetic Monte Carlo methods. *J. Comput. Aided Mater. Des.* **14**, 253 (2007).
49. S.J. Zhao, G.M. Stocks, and Y.W. Zhang: Defect energetics of concentrated solid-solution alloys from ab initio calculations: Ni_{0.5}Co_{0.5}, Ni_{0.5}Fe_{0.5}, Ni_{0.8}Fe_{0.2}, and Ni_{0.8}Cr_{0.2}. *Phys. Chem. Chem. Phys.* **18**, 24043 (2016).
50. S. Zhao, T. Egami, G.M. Stocks, and Y. Zhang: Effect of d electrons on defect properties in equiatomic NiCoCr and NiCrFeCr concentrated solid solution alloys. *Phys. Rev. Mater.* **2**, 013602 (2018).
51. W. Chen, X. Ding, Y. Feng, X. Liu, K. Liu, Z.P. Lu, D. Li, Y. Li, C.T. Liu, and X.-Q. Chen: Vacancy formation enthalpies of high-entropy FeCoCrNi alloy via first-principles calculations and possible implications to its superior radiation tolerance. *J. Mater. Sci. Technol.* **34**, 355 (2017).
52. S.C. Middleburgh, D.M. King, G.R. Lumpkin, M. Cortie, and L. Edwards: Segregation and migration of species in the CrCoFeNi high entropy alloy. *J. Alloy. Comp.* **599**, 179 (2014).
53. M.W. Ullah, D.S. Aidhy, Y. Zhang, and W.J. Weber: Damage accumulation in ion-irradiated Ni-based concentrated solid-solution alloys. *Acta Mater.* **109**, 17 (2016).
54. D. Chakraborty and D.S. Aidhy: Cr-induced fast vacancy cluster formation and high Ni diffusion in concentrated Ni-Fe-Cr alloys. *J. Alloy. Comp.* **725**(Suppl. C), 449 (2017).
55. L.K. Béland, C. Lu, Y.N. Osetskiy, G.D. Samolyuk, A. Caro, L. Wang, and R.E. Stoller: Features of primary damage by high energy displacement cascades in concentrated Ni-based alloys. *J. Appl. Phys.* **119**, 085901 (2016).
56. L.K. Béland, Y.N. Osetsky, and R.E. Stoller: The effect of alloying nickel with iron on the supersonic ballistic stage of high energy displacement cascades. *Acta Mater.* **116**, 136 (2016).
57. L. Koch, F. Granberg, T. Brink, D. Utt, K. Albe, F. Djurabekova, and K. Nordlund: Local segregation versus irradiation effects in high-entropy alloys: Steady-state conditions in a driven system. *J. Appl. Phys.* **122**, 105106 (2017).
58. S. Zhao, G. Velisa, H. Xue, H. Bei, W.J. Weber, and Y. Zhang: Suppression of vacancy cluster growth in concentrated solid solution alloys. *Acta Mater.* **125**, 231 (2017).

59. S. Zhao, Y. Osetsky, and Y. Zhang: Preferential diffusion in concentrated solid solution alloys: NiFe, NiCo, and NiCoCr. *Acta Mater.* **128**, 391 (2017).
60. Y.N. Osetsky, L.K. Béland, and R.E. Stoller: Specific features of defect and mass transport in concentrated fcc alloys. *Acta Mater.* **115**, 364 (2016).
61. G. Bonny, N. Castin, and D. Terentyev: Interatomic potential for studying ageing under irradiation in stainless steels: The FeNiCr model alloy. *Model. Simul. Mater. Sci. Eng.* **21**, 085004 (2013).
62. S. Zhao, Y.N. Osetsky, and Y. Zhang: Atomic-scale dynamics of edge dislocations in Ni and concentrated solid solution NiFe alloys. *J. Alloy. Comp.* **701**, 1003 (2017).
63. G. Veliša, E. Wendler, S. Zhao, K. Jin, H. Bei, W. Weber, and Y. Zhang: Delayed damage accumulation by athermal suppression of defect production in concentrated solid solution alloys. *Mater. Res. Lett.* **6**, 136 (2018).
64. A. Kohyama, A. Hishinuma, D.S. Gelles, R.L. Klueh, W. Dietz, and K. Ehrlich: Low-activation ferritic and martensitic steels for fusion application. *J. Nucl. Mater.* **233**, 138 (1996).
65. G. Veliša, M.W. Ullah, H. Xue, K. Jin, M.L. Crespillo, H. Bei, W.J. Weber, and Y. Zhang: Irradiation-induced damage evolution in concentrated Ni-based alloys. *Acta Mater.* **135**, 54 (2017).
66. K. Ming, X. Bi, and J. Wang: Precipitation strengthening of ductile $\text{Cr}_{15}\text{Fe}_{20}\text{Co}_{35}\text{Ni}_{20}\text{Mo}_{10}$ alloys. *Scripta Mater.* **137**, 88 (2017).
67. S. Gorsse, D.B. Miracle, and O.N. Senkov: Mapping the world of complex concentrated alloys. *Acta Mater.* **135**, 177 (2017).
68. D. Li, C. Li, T. Feng, Y. Zhang, G. Sha, J.J. Lewandowski, P.K. Liaw, and Y. Zhang: High-entropy $\text{Al}_{0.3}\text{CoCrFeNi}$ alloy fibers with high tensile strength and ductility at ambient and cryogenic temperatures. *Acta Mater.* **123**, 285 (2017).
69. Z. Li, K.G. Pradeep, Y. Deng, D. Raabe, and C.C. Tasan: Metastable high-entropy dual-phase alloys overcome the strength–ductility trade-off. *Nature* **534**, 227 (2016).
70. A.V. Kuznetsov, D.G. Shaysultanov, N.D. Stepanov, G.A. Salishchev, and O.N. Senkov: Tensile properties of an AlCrCuNiFeCo high-entropy alloy in as-cast and wrought conditions. *Mater. Sci. Eng., A* **533**, 107 (2012).
71. J.Y. He, H. Wang, H.L. Huang, X.D. Xu, M.W. Chen, Y. Wu, X.J. Liu, T.G. Nieh, K. An, and Z.P. Lu: A precipitation-hardened high-entropy alloy with outstanding tensile properties. *Acta Mater.* **102**, 187 (2016).

Supplementary Material

To view supplementary material for this article, please visit <https://doi.org/10.1557/jmr.2018.285>.